

Photoinduced collective motion of oil droplets and concurrent pattern formation in surfactant solution

Tomoya Kojima, Hiroyuki Kitahata, Kouichi Asakura, and Taisuke Banno*

[*] Tomoya Kojima, Prof. Kouichi Asakura, Dr. Taisuke Banno

Department of Applied Chemistry, Faculty of Science and Technology, Keio University, 3-14-1 Hiyoshi, Kohoku-ku, Yokohama, 223-8522, Japan

E-mail: banno@aplc.keio.ac.jp

Prof. Hiroyuki Kitahata

Department of Physics, Graduate School of Science, Chiba University, 1-33 Yayoi-cho, Inage-ku, Chiba 263-8522, Japan

Abstract

Collective motion is ubiquitous in living systems. Although various biomimetic artificial systems have been constructed, there have been few studies reported on collective motion induced by the coupling of chemical reactions, diffusion and convection in a far-from-equilibrium state. In this study, we report an artificial system of oil droplets in a surfactant solution wherein the collective motion of multiple droplets and pattern formation occurred concurrently. Using photo-responsive surfactants with an azobenzene moiety, the assembly of droplets and the formation of circular patterns around the formed droplet clusters occurred under UV illumination, whereas the disassembly of droplets and disappearance of the patterns occurred under subsequent visible light illumination. The observed dynamics were induced by Marangoni flows based on the reversible photoisomerisation of azobenzene-containing surfactants. The phenomena were considered analogous to the bioconvection of microorganisms. These findings could be useful for understanding the mechanism of motion of life in terms of physicochemical aspects.

Introduction

Motion is one of the essential dynamics for characterising life. To approach the essence of motion in living systems, microorganisms have been utilised as models. They respond to external stimuli and change their mode of motion. For example, the cellular slime mould *Dictyostelium discoideum* and the nematode *Caenorhabditis elegans* exhibit taxis in response to chemicals^{1,2}, light^{3,4}, electricity^{5,6}, and temperature^{7,8}. Alga *Chlamydomonas*⁹ and *Euglena*¹⁰ with flagella also show taxis to light irradiation, and the positive and negative modes are switchable depending on the intensity. Moreover, they generate bioconvection as collective behaviour owing to their individual phototaxis and the surrounding hydrodynamic effect, resulting in the formation of a macroscopic ordered pattern^{11,12}. Various reductive and constructive approaches have revealed that the characteristic dynamics of microorganisms are induced by hierarchical chemical reaction networks^{13–15}. However, the mechanisms have not yet been fully elucidated owing to their complexity. Therefore, the construction of simpler artificial systems that reproduce the characteristic behaviour of organisms would allow us to consider complicated living systems as physicochemical phenomena¹⁶.

Thus far, various artificial objects that transduce chemical energy from external stimuli to their own mechanical energy have been created^{17–21}. Solid anisotropic particles, that is, Janus particles, exhibit directional motion induced by light irradiation²², electric field²³, decomposition of H₂O₂²⁴, and thermal gradient²⁵. Liquid droplets perform programmed motion, including directional motion and simple tasks in response to light^{26–29}, temperature³⁰, pH^{31–33}, salt concentration³⁴, and metal ions^{35,36}. In addition, the collective motion of solid particles without anisotropy emerged owing to electric-field-induced fluid flows³⁷ and the diffusiophoresis of ions that are generated by the photodecomposition of metal particles³⁸. Motion of droplets induced by the dissolution of droplets has also been demonstrated^{39–43}. Despite considerable progress made to date, no examples of more complicated biomimetic systems have been reported where the directional motion of objects induces other macroscopic dynamics, such as collective motion and pattern formation, triggered by a coupling of chemical reactions, diffusion and convection.

Thus, we herein report an artificial system wherein the convection of oil droplets exhibiting taxis is associated with their collective motion. The main driving force of moving liquid droplets in a surfactant solution is estimated to be Marangoni flows based on the

heterogeneity in the interfacial tension at the droplet surface^{44–45}. To construct the targeted system, we focused on photo-responsive surfactants with an azobenzene moiety (AzoTAB, Fig. 1a) because the use of light as an external stimulus has the advantage of fine control of the position and area. Some studies have previously reported that photoisomerisation of azobenzene-containing surfactants between *trans*- and *cis*-isomers induces Marangoni flows due to local changes in the interfacial tension of the droplet surface, resulting in the taxis of droplets^{26,29}. Therefore, by using AzoTAB, we expected that specific convection around each oil droplet exhibiting taxis was generated, inducing the collective motion of multiple droplets.

Results and Discussion

The dynamics of the oil droplets in a surfactant solution under light illumination were observed. The observation sample was prepared by gently mixing 4.3 μL of heptyloxybenzaldehyde (HBA) with 85.7 μL of 50 mM mixed solution, including azobenzene-containing surfactant (AzoTAB) and dodecyltrimethylammonium bromide (DTAB) at the equivalent molar ratio (Figure 1a). The dispersions were poured into a pool-like sealed chamber (Figure 1b) and observed under a phase-contrast microscope. Droplets with diameters in the range of 5–170 μm (Figure S1) were observed, and their motion time when all droplets ceased their motion in the chamber was 13 ± 3 min on an average of 10 trials. Because the density of oil and the surfactant solution was 0.99 and nearly 1.0 respectively, droplets were in the vicinity of an upper cover slip in the chamber due to buoyancy when they ceased the motion. Next, we performed a light-illumination experiment for 180 s for each trial. When the dispersion was illuminated with UV light at 1.2 mW/cm^2 for 180 s from the upper side, droplets started to move to the lower side and gradually assembled with each other (Figure 1c and Supplementary Movie S1). Note that, immediately after UV illumination, the droplets moved slightly against UV in the lateral direction for a few seconds because the emulsion was not illuminated from the vertical upper side, but from the diagonal upper side. After assembly, circular patterns around each droplet cluster gradually appeared. Hydrophobic and hydrophilic fluorescent dyes, 5-FITC, Nile Red, Rhodamine 6G, Rhodamine B, and Uranine, accumulated in line with the patterns (Figure S2). The patterns were larger with the size of the clusters (Figure S3). Under the subsequent visible (vis) light illumination at 5.8 mW/cm^2 , droplets in the clusters disassembled, and the circular patterns disappeared

(Figure 1c and Supplementary Movie S2). We considered a series of assembly and disassembly dynamics of droplets under light illumination as the collective motion coupled with phototaxis. The time course of the height of the oil droplets was observed (Figure S4). The oil droplets first moved downward under UV illumination. Smaller droplets tended to rapidly move upward when they approached the other droplets and formed a cluster. After UV illumination for 180 s, each droplet in a cluster was almost in contact with the upper cover slip (Figure S5 and Table S1). Under vis illumination, all the observed droplets did not change their height significantly and remained near the upper cover slip. The collective motion and pattern formation were observed repeatedly under UV illumination for 180 s and subsequent vis illumination for 180 s, alternated three times (Figure S6). When the intensity of light was higher, the same phenomena were observed under UV illumination (Figure S7). In contrast, disassembly behaviour depended on the intensity of the vis light: the stronger the illumination was, the more the oil droplets were dispersed (Figure S8). The dynamics were also influenced by the thickness of the chamber (Figure S9). Collective motion was clearly observed when the thickness was greater than 160 μm . These results suggest that the photoinduced dynamics depend on the experimental conditions.

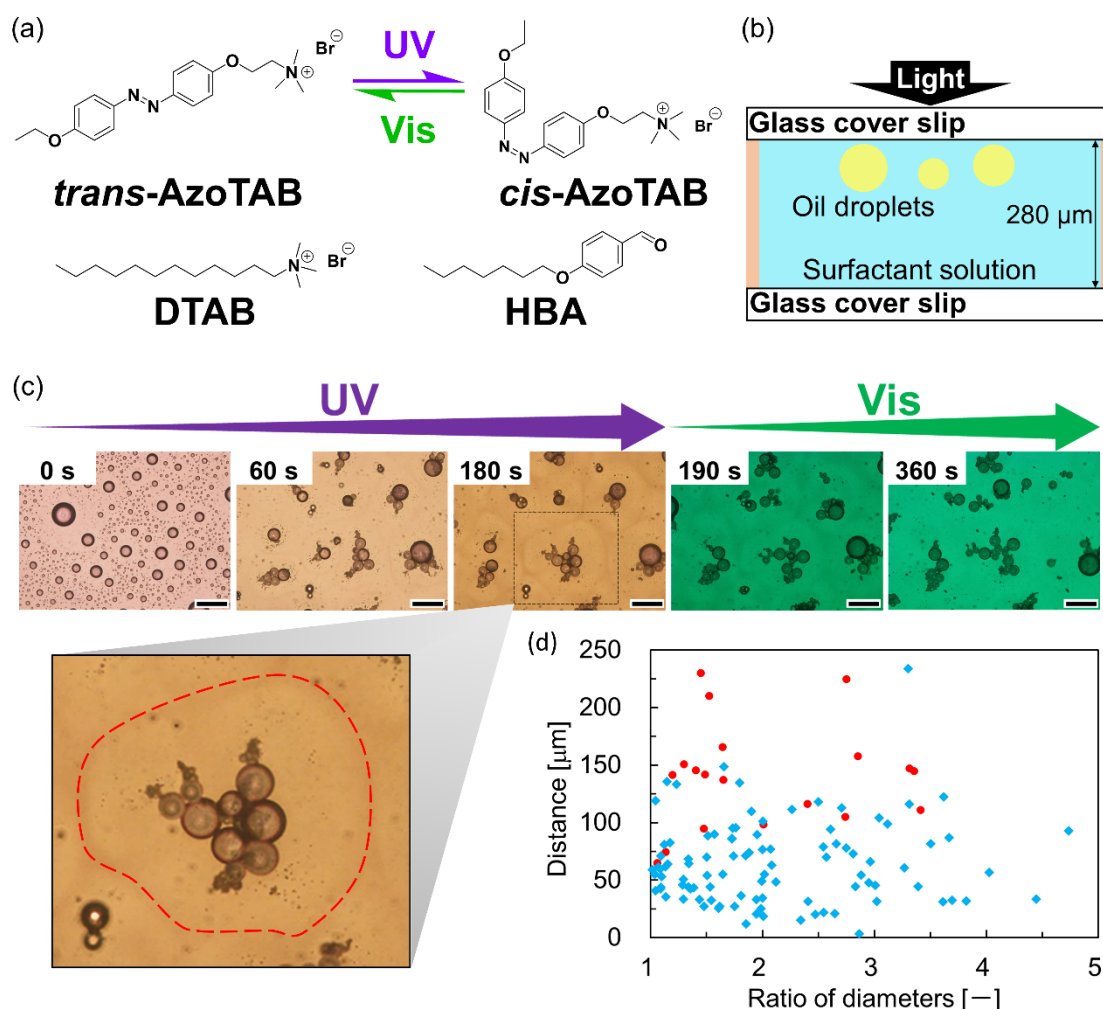


Figure 1. Collective motion of droplets and pattern formation. **(a)** Chemical structures of surfactants and oil. **(b)** A pool-like sealed chamber with the depth of 280 μm used in the microscope observation. The chamber was illuminated with light from the upper side. **(c)** Typical sequential micrographs of HBA droplets in 50 mM AzoTAB/DTAB (50/50 mol%) solution under light illumination. Dotted red line in an enlarged micrograph represents one of the patterns. Scale bar: 200 μm . **(d)** Observation results of the initial distance between two droplets and the ratio of their diameters. Blue and red symbols indicate occurrence and no occurrence of assembly dynamics, respectively.

Focusing on the assembling behaviour of oil droplets under UV illumination, the threshold of the distance was investigated. To exclude the influence of the lateral motion observed immediately after UV illumination, the distance between two droplets was determined after the droplets ceased lateral motion. From the relationship between the ratio of diameters and distance between two droplets, the threshold of the distance for the occurrence of assembly was confirmed to be approximately 100 μm regardless of the difference in the diameters. (Figure 1d). In the emulsion with a lower number density of droplets prepared using a smaller amount of HBA, a similar threshold was observed (Figure S10a). In addition, no difference was observed in the threshold under UV illumination with a higher intensity (Figure S10b). These results clearly indicate that the assembly of droplets under UV illumination depends on the distance between droplets.

To clarify the mechanism by which both the collective behaviour of droplets and pattern formation emerged, we first investigated the photoisomerisation of AzoTAB by UV-vis spectroscopy. A 50 mM AzoTAB/DTAB (50/50 mol%) solution without HBA which was illuminated with light was diluted and measured. The *cis*-isomer ratio was calculated using the calibration curve, which was based on the absorbance at 357 nm, the maximum absorption wavelength of the *trans*-isomer (Figures S11a and b). Given that the half-life of AzoTAB from its *cis*- to *trans*-isomer was estimated to be 13 h (Figure S11c), spontaneous isomerisation was negligible under the tested conditions. The isomerisation from the *trans*- to *cis*-isomer gradually occurred under UV illumination, whereas reverse photoisomerisation occurred under vis illumination (Figure 2a). Further, the isomerisation rate increased as the intensity of the light increased (Figure S12).

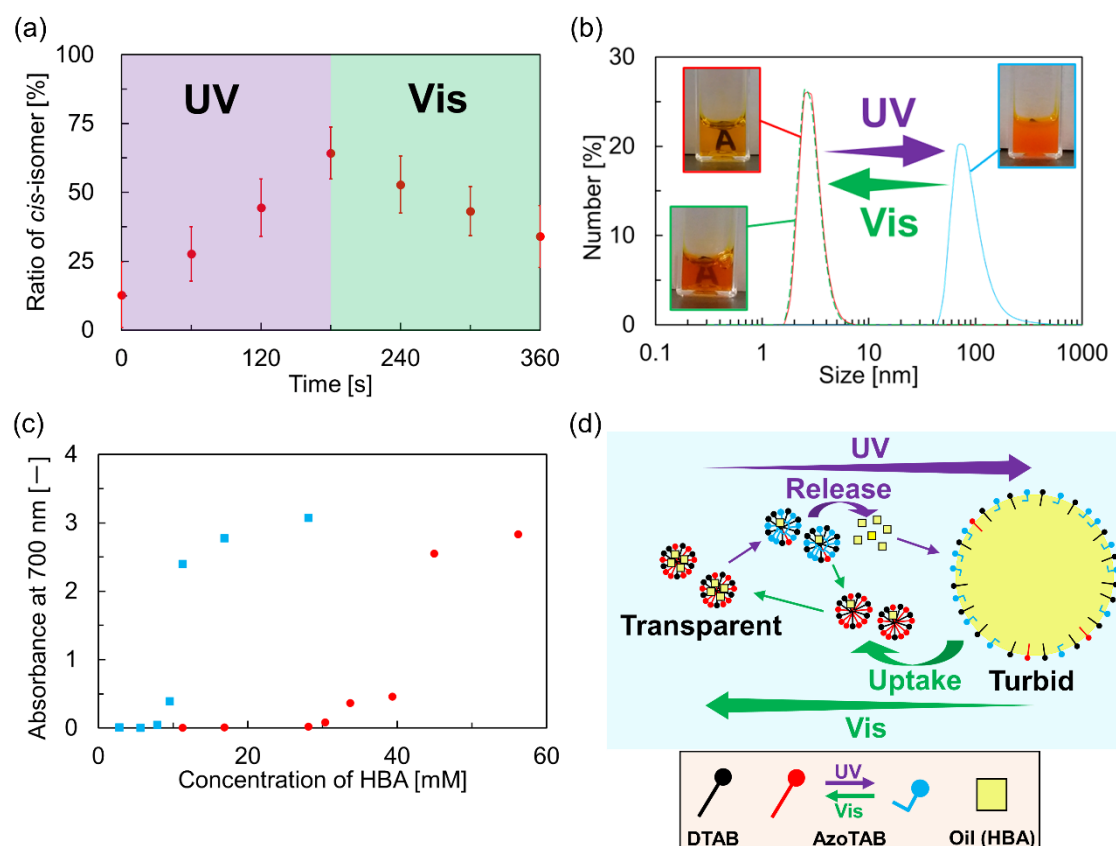


Figure 2. Surfactant properties of AzoTAB before and after light illumination. **(a)** Time-course of the isomerisation ratio of AzoTAB in 50 mM AzoTAB/DTAB (50/50 mol%) solution under UV and subsequent vis illumination. **(b)** Size distribution of nanoparticles of filtrates before (red) and after UV illumination (blue), and after subsequent vis illumination (dotted green) analysed by dynamic light scattering. Turbidity of filtrates observed by the naked eye is shown in insets. As the paper where the letter “A” is placed behind the cell, the letter “A” can be viewed if the filtrate is transparent. **(c)** Relationship between absorbance at 700 nm and concentration of HBA per 50 mM AzoTAB/DTAB (50/50 mol%) solution when AzoTAB was *trans*-isomer rich (red) and *cis*-isomer rich (blue). **(d)** Schematic representation of change at a nanometre scale.

Next, we examined the change in surfactant properties by the photoisomerisation of AzoTAB under UV and vis illumination. According to surface tension measurements by the pendant drop method, the critical micelle concentration (CMC) of AzoTAB and DTAB mixed in the equivalent molar ratio when AzoTAB was *trans*-isomer rich or *cis*-isomer rich was determined. Before the measurements, the *cis*-isomer ratio of AzoTAB in the *cis*-isomer-rich solution was confirmed to be more than 90%. The CMC was 15 mM and 16 mM for the *trans*-isomer-rich and *cis*-isomer-rich solutions, respectively (Figure S13a). In addition, the diameter of the micelles in both the 50 mM *trans*-AzoTAB-rich solution and *cis*-AzoTAB-rich solution was a few nanometres according to the dynamic light scattering (DLS) method (Figure S13b). We also measured the particle diameter in 50 mM AzoTAB/DTAB (50/50 mol%) solution containing HBA after filtration using a 0.8 μm syringe filter. The DLS measurements showed that the diameters before and after UV illumination were 3 nm and 70 nm, respectively (Figure 2b). Under subsequent vis illumination, the size distribution returned to its original value. This result was in accordance with observations of the filtrate by the naked eye (Figure 2b insets). The filtrate was initially transparent, and it became turbid under UV illumination and then returned to transparent under subsequent vis illumination. To estimate the maximum amount of solubilised HBA in micelles that included much *trans*- or *cis*-AzoTAB, we measured the absorbance intensity at 700 nm, where the peak from AzoTAB, DTAB, and HBA was not detected, as a barometer of turbidity at room temperature. The maximum solubilised amount was estimated to be the oil volume when the absorbance intensity increased, indicating that the mixture became turbid. The relative ratio of the solubilised amount into micelles was 3.6 to 1.0, as observed in Figure 2c. Based on these results, due to the photoisomerisation of AzoTAB, HBA was released from the micelles, and larger particles were generated under UV illumination. Meanwhile, HBA was resolubilised into the micelles under subsequent vis illumination (Figure 2d).

In addition, the effect of AzoTAB isomerisation on the interfacial tension between the AzoTAB/DTAB (50/50 mol%) solution and HBA was investigated using the drop weight method. The interfacial tension of the solution containing a large amount of *trans*-isomer (>90%) was higher than that containing a large amount of *cis*-isomer (>90%) at the tested concentrations (Figure 3a). Therefore, it was considered that the interfacial tension between the oil and surfactant solution became higher or lower under UV or vis illumination,

respectively, owing to the photoisomerisation of AzoTAB. Thus, we observed the interface between 50 mM AzoTAB/DTAB (50/50 mol%) solution and HBA in a glass vial when the specimen was illuminated with UV from the right side (Figures 3b–c and Supplementary Movie S3). Convective flows from the left to the right side at the interface generated in each phase immediately after UV illumination. Because the interfacial tension increased owing to the photoisomerisation of AzoTAB from the *trans*- to *cis*-isomer, it was suggested that the interfacial tension of the illuminated side was higher than that of the non-illuminated side, inducing Marangoni flows from the area with lower interfacial tension to that with the higher one. Based on these results, it was clarified that the photoisomerisation of AzoTAB caused a difference in the interfacial tension that was sufficient for inducing Marangoni flows at the interface.

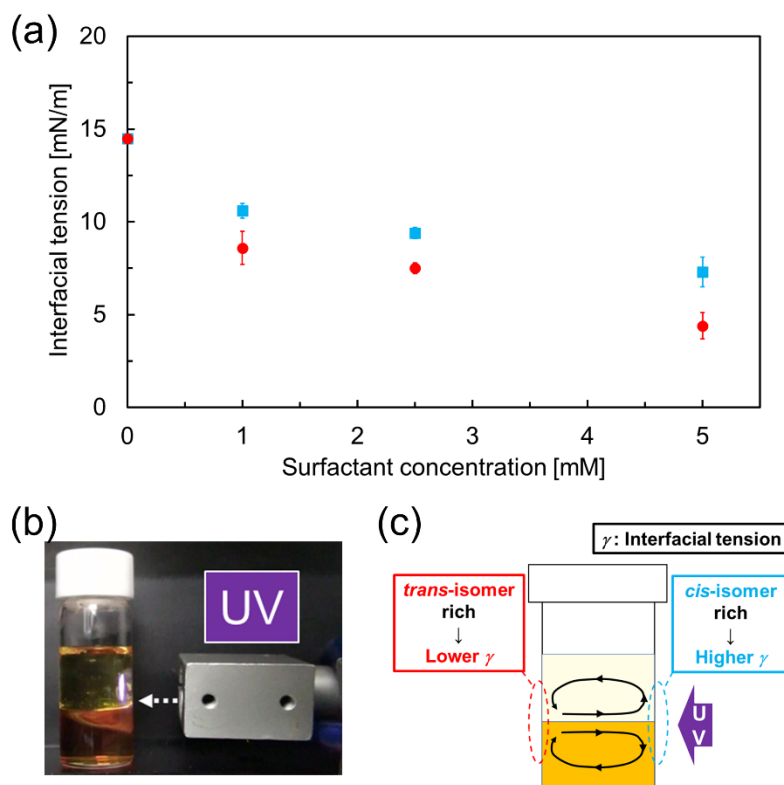


Figure 3. Variation in the interfacial tension along the photoisomerisation of AzoTAB. **(a)** Interfacial tension between AzoTAB/DTAB (50/50 mol%) solution containing >90% *trans*-isomer (red) or >90% *cis*-isomer (blue) and HBA with the surfactant concentration according to the pendant drop method at room temperature. **(b)** Experimental setup of equipment. **(c)** Schematic representation of the observation of convective flows induced at the interface between 50 mM surfactant solution (lower phase) and HBA (upper phase).

Thus, we attempted to visualise the flow fields around the clusters of oil droplets induced by the photoisomerisation of AzoTAB using polyethylene fluorescent beads with a diameter of 10–22 μm . Because the density of the beads was 0.998 g/cm^3 and lower than that of the surfactant solution, which was nearly equal to 1.0 g/cm^3 , the beads floated near the upper cover slip. It was observed that the beads moved radially from a droplet cluster and accumulated in line with circular patterns (Figures 4a–b and Supplementary Movie S4). A few beads moved in the z-direction. The beads rose to the upper cover slip near the droplet cluster and went down in the area where the circular pattern was generated (Figure 4c and Supplementary Movie S5). This indicates that the variation of interfacial tension of the droplet surface by the photoisomerisation of AzoTAB induced convective flows between two areas where droplet clusters and circular patterns formed. Under vis illumination, the bead moved with circulating around a droplet cluster in the x–z plane (Figure 4d and Supplementary Movies S6 and S7). However, the observed motion was similar to that under UV illumination, especially with respect to the way of the circulation. The speed of the bead under both UV and vis illumination was 2–5 $\mu\text{m}/\text{s}$, but rose temporarily to approximately 10 $\mu\text{m}/\text{s}$ when the bead was close to the droplet cluster (Figures S14–S16). Thus, we estimated the characteristic thresh speed induced by droplet clusters from the speed of the fluorescent beads. The Reynolds number Re equals $\rho vL/\eta$, where ρ is the density, v is the speed, L is the diameter, and η is the viscosity constant. Because the Reynolds number Re was 10^{-5} – $10^{-4} \ll 1$ when $\rho = 0.998 \text{ g}/\text{cm}^3$, $v = 2$ – $12 \mu\text{m}/\text{s}$, $L = 10$ – $22 \mu\text{m}$, and $\eta = 0.89 \text{ mPa}\cdot\text{s}$, Stokes' law was applicable. Since the resistance force is estimated from the Stokes resistance $6\pi\eta rv$, where η is the viscosity constant, r is the radius, and v is the speed, it was calculated that under UV and vis illumination, the force was around 0.1–2.0 pN (Figures S14–S16).

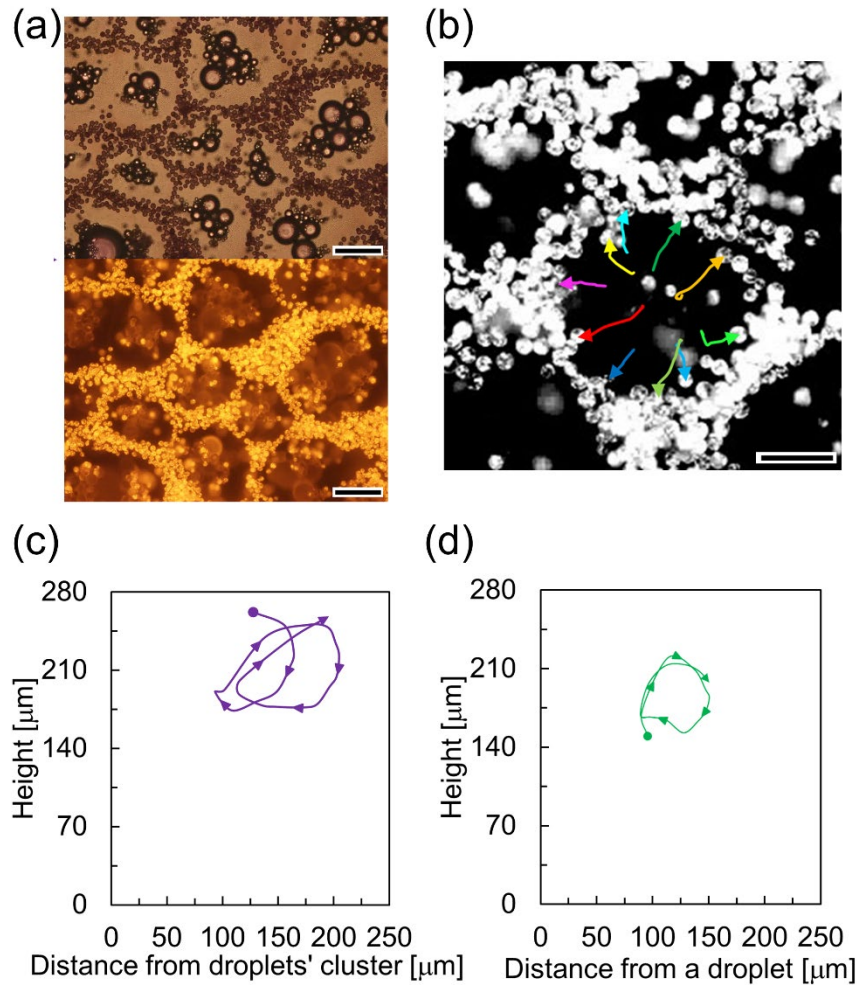


Figure 4. Visualisation of flow fields around the droplets' cluster. **(a)** Bright field (top) and fluorescent (bottom) images of HBA droplets in 50 mM AzoTAB/DTAB (50/50 mol%) surfactant solution 3 min after UV illumination (excitation: 530–550 nm, emission: 570– nm). Scale bar: 200 μm . **(b)** Trajectories of 10 fluorescence beads represented by arrows near the upper cover slip under UV illumination. These beads were accumulated in line with a circular pattern. Scale bar: 100 μm . **(c)** Trajectory of a bead moving in the x – z plane under UV illumination. The circle and arrow represent the initial and end position, respectively. **(d)** Trajectory of a bead moving with circulating in the x – z plane under vis illumination. The circle and arrow represent the initial and end position, respectively.

Because no significant difference in the flow direction was confirmed under UV and vis illumination, we investigated the influence of the absorption of light by oil on the photoisomerisation of AzoTAB at the droplet surface. At around 365 nm, in the UV region, HBA was mostly not able to transmit UV (Figure S17). This indicates that the photoisomerisation from the *trans*- to *cis*-isomer mainly occurred at the illuminated upper side of the oil droplets (Figure 5a). On the other hand, at around 480 nm, in the vis region, HBA almost completely transmitted light (Figure S17), indicating that the photoisomerisation from the *cis*- to the *trans*-isomer of AzoTAB occurred not only on the illuminated side but also on the opposite side of the droplet surface. The interpretation suggested that heterogeneity in the interfacial tension at the droplet surface, which is dominant for self-propelled motion, was not generated. However, this contradicts the observed results. Thus, we focused on the light refraction based on Snell's law. Since the refractive index of HBA and the surfactant solution were 1.52 and 1.33, respectively, vis light could be refracted and condensed at the lower side of the oil droplets, as if the oil droplets behaved as a lens (Figure 5b). The analysis by Snell's law suggested that the area illuminated with refracted vis light at the lower side was smaller than the area illuminated directly at the upper side, indicating that the strength of the illuminated light per unit surface area was stronger at the lower side. Thus, the interfacial tension at the lower side of the droplet became lower than that at the upper side because of faster photoisomerisation from the *cis*- to the *trans*-isomer of AzoTAB. Given that the middle area of the droplet was weakly illuminated with vis light due to light refraction, the photoisomerisation of AzoTAB occurred slowly. This indicates that the interfacial tension at the middle area was higher than at the top or bottom. In summary, Marangoni flows were considered to be induced higher from the bottom to middle than from the top to the middle of the droplet. Such quadrupolar flows around each droplet likely induced the disassembly of the droplets. Mathematical simulations based on hydrodynamics considering the interfacial tension gradient due to the photoisomerization at the droplet boundary supported the generation of such flows under UV illumination (Figure 5c) and vis illumination (Figure 5d).

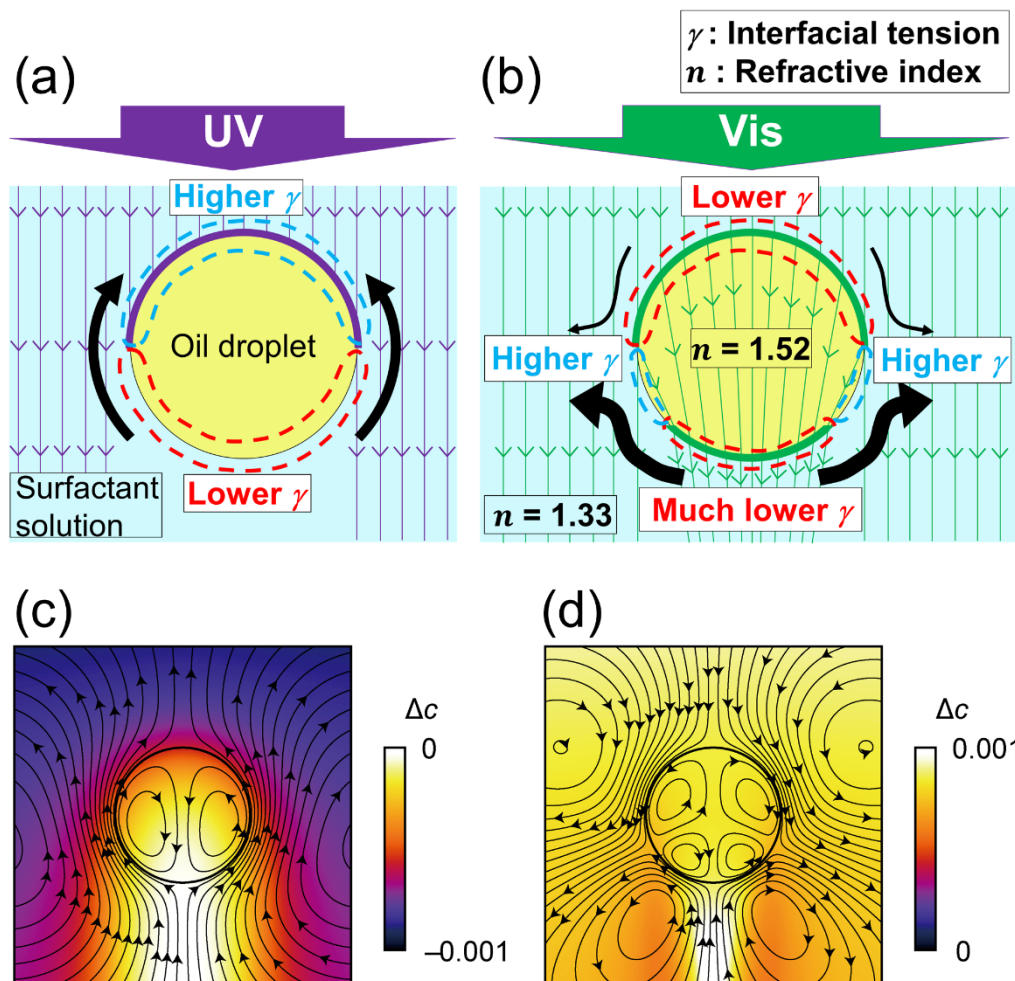


Figure 5. Schematic representations of illuminated light toward an oil droplet, thereby inducing Marangoni flows under UV illumination (a) and vis illumination (b). Italic character n represents a refractive index. Results of mathematical simulations corresponding to the system with a single oil droplet under UV illumination (c) and vis illumination (d). The profiles of the difference in concentration field of *trans*- and *cis*-isomers are shown in the colour code and the flow profile is shown as streamlines.

Based on the flow fields induced by the photoisomerisation of AzoTAB, a mechanism for the collective behaviour of oil droplets and concurrent pattern formation was proposed. Under UV illumination, the behaviour can be classified into three stages. In the first stage, as the photoisomerisation from the *trans*- to the *cis*-isomer of AzoTAB occurred, the droplet surface of the UV-illuminated side increased the interfacial tension due to the UV absorption of the HBA droplet. Therefore, the Marangoni flows moving upwards, generated by the gradient of interfacial tension, induced the negative phototaxis of the droplet to the bottom (Figure 6a). In the second stage, droplets moved toward each other, inducing assembly (Figure 6b). Circulating convection generated around each droplet because of the above-mentioned Marangoni flows. Surfactants were transported constantly by the convection. When two droplets were close to a certain degree, the convection around each droplet transported and concentrated surfactants at the intermediate region between droplets. Then, the interfacial tension of the oil droplet at the side facing another one got lower than at the opposite side. This resulted in the formation of lateral gradient of interfacial tension, inducing Marangoni convection which drove each droplet toward each other. Therefore, to form the surfactant-rich region by the circulating convection around each droplet, the threshold of the distance for the occurrence of assembly existed (Figure 1d). Mathematical simulation supported that the lateral gradient of surfactants appeared as two droplets got closer (Figure S18). In the third stage, owing to the difference in the maximum solubilised amount between *trans*- and *cis*-AzoTAB, oil was released from the micelles, and the larger particles formed under UV illumination. The particles were swept away by convection around the droplet clusters (Figure 6c). Because convection was induced around the droplet clusters in any direction, the particles accumulated in the shape of circles, resulting in circular patterns appearing around the droplet clusters (Figure 6d).

On the other hand, under *vis* illumination, considering the light transmittance and refraction of oil droplets, photoisomerisation from the *cis*- to the *trans*-isomer of AzoTAB proceeded. Therefore, the droplet surface at both the upper and bottom sides experienced an increase in interfacial tension, compared to the middle area. Such a gradient of interfacial tension induced Marangoni flow from the bottom to the middle and from the top to the middle of the droplets. The formed quadrupolar flows around each droplet repelled each other, resulting in disassembly (Figure 6e). In addition, as photoisomerisation of AzoTAB from the

cis- to the *trans*-isomer caused micelles to incorporate more oil, the particles that were accumulated at the patterns resolubilised into micelles, indicating the disappearance of the patterns (Figures 6f–g).

So far, the collective behaviour under far-from-equilibrium conditions has been observed in not only microorganisms^{46,47} but also artificial objects^{48,49}. For instance, if the distance between two droplets on a glass is below the critical value, they spontaneously approach each other due to Marangoni contraction^{50,51}. On the other hand, the photoinduced collective behaviour of droplets was induced by the obvious hierarchical structure composed of chemical reactions, diffusion, and convection. We thus consider that the current finding provides a new aspect for design and induction of life-like complex behaviour in terms of molecular chemistry.

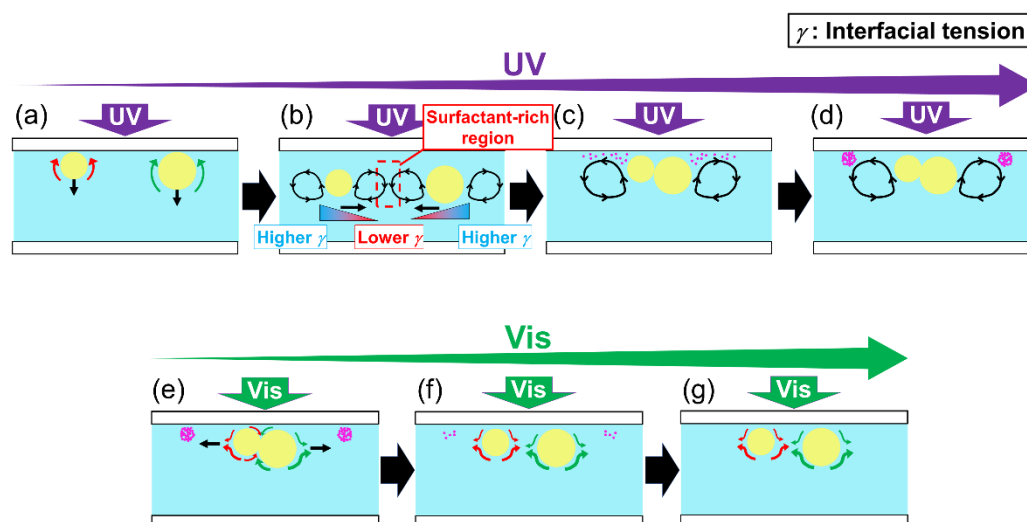


Figure 6. Schematic illustration of the proposed mechanism for collective behaviour of oil droplets and pattern formation. Under UV illumination, **(a)** oil droplets moved to the bottom. **(b)** Droplets moved toward each other, inducing assembly. **(c)** Oil particles (magenta) caused by solubilised oil released from micelles gradually generated due to the photoisomerisation of AzoTAB. **(d)** Finally, the particles were swept away by convection around droplets' clusters and accumulated at the point where the convection sank, forming circular patterns. Under vis illumination, **(e)** droplets repelled each other due to the formed convection around each droplet. **(f)** Oil particles accumulated at the patterns were incorporated into micelles and decreased. **(g)** The patterns that resulted from the oil particles disappeared.

Conclusion

We have demonstrated an artificial system wherein the collective motion of multiple droplets and concurrent pattern formation emerged from the coupling of chemical reactions, diffusion and convection. By using photo-responsive azobenzene-containing surfactants, the assembly of droplets and the formation of circular patterns around the formed droplet clusters were observed under UV illumination. In addition, under subsequent vis illumination, the disassembly of droplets and disappearance of the patterns occurred. It was revealed that changes in interfacial tension were due to the photoisomerisation of AzoTAB, which induced the phototaxis of the droplets and generated characteristic convection. Mathematical simulations based on hydrodynamics supported the generation of such flows. The convection around each droplet caused them to assemble under UV illumination, whereas they disassembled under vis illumination. In addition, a significant difference in the change in the maximum solubilised oil amount in the micelles was observed between *trans*- and *cis*-AzoTAB. This suggests the induced release of the oil component from micelles under UV illumination and the incorporation into micelles under vis illumination. Thus, the released oil components were swept away by convection and accumulated, resulting in circular patterns under UV illumination. In contrast, vis illumination resulted in the disappearance of circular patterns due to the resolubilisation of oil components into micelles. Our findings were considered to be analogous to the bioconvection of microorganisms inducing the assembly of many individuals and formation of macroscopic patterns^{11,12}. Therefore, this study could be a useful model for understanding the mechanism of collective motion in life in terms of physicochemical aspects.

Acknowledgments

Mr. Tsuneyoshi Torii and Ms. Mitsuyo Matsubara (Malvern Panalytical, a division of Spectris Co. Ltd.) is acknowledged for the measurements of ζ potentials. We would like to thank Editage (www.editage.com) for English language editing. This work was supported by JSPS KAKENHI Grant Number 18K05066 for T.B.

Author contributions

T. K. and T. B. designed the experiments. T. K. performed the experiments. H. K. analysed the data and performed mathematical simulation. T. K., H. K., K. A., and T. B. discussed the results. T. K., H. K., and T. B. wrote the manuscript.

Competing interests

The authors declare no competing interests.

References

1. Hong, C. B., Häder, M. A. & Häder, D-P. Phototaxis in *Dictyostelium discoideum* amoebae. *Photochem. Photobiol.* **33**, 373–377 (1980).
2. Pierce-Shimomura, J. T., Morse, T. M. & Lockery, S. R. The Fundamental Role of Pirouettes in *Caenorhabditis elegans* Chemotaxis. *J. Neurosci.* **19**, 9557–9569 (1999).
3. Iijima, M., Huang, Y. E. & Devreotes, P. Temporal and spatial regulation of chemotaxis. *Dev. Cell* **3**, 469–478 (2002).
4. Ward, A., Liu, J., Feng, Z. & Xu, X. Z. S. Light-sensitive neurons and channels mediate phototaxis in *C. elegans*. *Nat. Neurosci.* **11**, 916–922 (2008).
5. Zhao, M., Jin, T., McCaig, C. D., Forrester, J. V. & Devreotes, P. N. Genetic analysis of the role of G protein-coupled receptor signaling in electrotaxis. *J. Cell Biol.* **157**, 921–927 (2002).
6. Sukul, N. C. & Croll, N. A. Influence of potential difference and current on the electrotaxis of *Caenorhabditis elegans*. *J. Nematol.* **10**, 814–817 (1978).
7. Whitaker, B. D. & Poff, K. L. Thermal adaptation of thermosensing and negative thermotaxis in *Dictyostelium*. *Exp. Cell Res.* **128**, 87–93 (1980).
8. Hedgecock, E. M. & Russell, R. L. Normal and mutant thermotaxis in the nematode *Caenorhabditis elegans*. *PNAS* **72**, 4061–4065 (1975).
9. Feinleib, M. E. H. & Curry, G. M. The relationship between stimulus intensity and oriented phototactic response (topotaxis) in *Chlamydomonas*. *Physiol. Plant.* **25**, 346–352 (1971).
10. Häder, D-P., Colombetti, G., Lenci, F. & Quaglia, M. Phototaxis in the Flagellates,

- Euglena gracilis* and *Ochromonas Danica*. *Arch. Microbiol.* **130**, 78–82 (1981).
11. Suematsu, N. J., et al. Localized bioconvection of *Euglena* caused by phototaxis in the lateral direction. *J. Phys. Soc. Jpn.* **80**, 064003 (2011).
 12. Williams, C. R. & Bees, M. A. A tale of three taxes: photo-gyro-gravitactic bioconvection. *J. Exp. Biol.* **214**, 2398–2408 (2011).
 13. Van Haastert, P. J. M. & Devreotes, P. N. Chemotaxis: signalling the way forward. *Nat. Rev. Mol. Cell Biol.* **5**, 626–634 (2004).
 14. Bargmann, C. I. *Chemosensation in C. elegans* (The *C. elegans* Research Community, WormBook, 2006).
 15. Sineshchekov, O. A., Jung, K. & Spudich, J. L. Two rhodopsins mediate phototaxis to low- and high-intensity light in *Chlamydomonas reinhardtii*. *PNAS* **99**, 8689–8694 (2002).
 16. Suematsu, N. J. & Nakata, S. Evolution of self-propelled objects: from the viewpoint of nonlinear science. *Chem. Eur. J.* **24**, 6308–6324 (2018).
 17. Tu, Y., et al. Motion control of polymeric nanomotors based on host–guest interactions. *Angew. Chem. Int. Ed.* **58**, 8687–8691 (2019).
 18. Uchida, E., Azumi, R. & Norikane, Y. Light-induced crawling of crystals on a glass surface. *Nat. Commun.* **6**, 7310 (2015).
 19. Nakata, S., Miyaji, T., Matsuda, Y., Yoshii, M. & Abe, M. Mode switching of a self-propelled camphor disk sensitive to the photoisomerization of a molecular layer on water. *Langmuir* **30**, 7353–7357 (2014).
 20. Ikegami, T., Kageyama, Y., Obara, K. & Takeda, S. Dissipative and autonomous square-wave self-oscillation of a macroscopic hybrid self-assembly under continuous light irradiation. *Angew. Chem. Int. Ed.* **55**, 8239–8243 (2016).
 21. Wang, H. & Pumera, M. Fabrication of micro/nanoscale motors. *Chem. Rev.* **115**, 8704–8735 (2015).
 22. Chen, C., et al. Light-steered isotropic semiconductor micromotors. *Adv. Mater.* **29**, 1603374 (2017).
 23. Gangwal, S., Cayre, O. J., Bazant, M. Z. & Velev, O. D. Induced-charge electrophoresis of metallodielectric particles. *Phys. Rev. Lett.* **100**, 058302 (2008).
 24. Paxton, W. F., et al. Catalytic nanomotors: autonomous movement of striped nanorods. *J. Am. Chem. Soc.* **126**, 13424–13431 (2004).
 25. Xuan, M., et al. Near infrared light-powered Janus mesoporous silica nanoparticle motors. *J. Am. Chem. Soc.* **138**, 6492–6497 (2016).
 26. Diguët, A., et al. Photomanipulation of a droplet by the chromocapillary effect. *Angew. Chem. Int. Ed.* **48**, 9281–9284 (2009).
 27. Florea, L., et al. Photo-chemopropulsion – Light-stimulated movement of microdroplets.

- Adv. Mater.* **26**, 7339–7345 (2014).
28. Suzuki, K. & Sugawara, T. Phototaxis of oil droplets comprising a caged fatty acid tightly linked to internal convection. *ChemPhysChem* **17**, 2300–2303 (2016).
 29. Kaneko, S., Asakura, K. & Banno, T. Phototactic behavior of self-propelled micrometer-sized oil droplets in a surfactant solution. *Chem. Commun.* **53**, 2237–2240 (2017).
 30. Ichikawa, M., Takabatake, F. & Miura, K. Controlling negative and positive photothermal migration of centimeter-sized droplets. *Phys. Rev. E* **88**, 012403 (2013).
 31. Hanczyc, M. M., Toyota, T., Ikegami, T., Packard, N. & Sugawara, T. Fatty acid chemistry at the oil–water interface: self-propelled oil droplets. *J. Am. Chem. Soc.* **129**, 9386–9391 (2007).
 32. Lagzi, I. Soh, S., Wesson, P. J., Browne, K. P. & Grzybowski, B. A. Maze solving by chemotactic droplets. *J. Am. Chem. Soc.* **132**, 1198–1199 (2010).
 33. Miura, S., et al. pH-induced motion control of self-propelled oil droplets using a hydrolyzable gemini cationic surfactant. *Langmuir* **30**, 7977–7985 (2014).
 34. Čejková, J., Novák, M., Štěpánek, F. & Hanczyc, M. M. Dynamics of chemotactic droplets in salt concentration gradients. *Langmuir* **30**, 11937–11944 (2014).
 35. Ban, T., Tani, K., Nakata, H. & Okano, Y. Self-propelled droplets for extracting rare-earth metal ions. *Soft Matter* **10**, 6316–6320 (2014).
 36. Ban, T. & Nakata, H. Metal-ion-dependent motion of self-propelled droplets due to the Marangoni effect. *J. Phys. Chem. B* **119**, 7100–7105 (2015).
 37. Yeh, S., Seul, M. & Shraiman, B. I. Assembly of ordered colloidal aggregates by electric-field-induced fluid flow. *Nature* **386**, 57–59 (1997).
 38. Ibele, M., Mallouk, T. E. & Sen, A. Schooling behavior of light-powered autonomous micromotors in water. *Angew. Chem. Int. Ed.* **48**, 3308–3312 (2009).
 39. Thutupalli, S., Seemann, R. & Herminghaus, S. Swarming behavior of simple model squirmers. *New J. Phys.* **13**, 073021 (2011).
 40. Thutupalli, S., Geyer, D., Singh, R., Adhikari, R. & Stone, H. A. Flow-induced phase separation of active particles is controlled by boundary conditions. *PNAS* **115**, 5403–5408 (2018).
 41. Tanaka, S., Nakata, S. & Kano, T. Dynamic ordering in a swarm of floating droplets driven by solutal Marangoni effect. *J. Phys. Soc. Jpn.* **86**, 101004 (2017).
 42. Čejková, J., Schwarzenberger, K., Eckert, K. & Tanaka, S. Dancing performance of organic droplets in aqueous surfactant solutions. *Colloids Surf. A* **566**, 141–147 (2019).
 43. Krüger, C., Bahr, C., Herminghaus, S. & Maass, C. C. Dimensionality matters in the collective behaviour of active emulsions. *Eur. Phys. J. E* **39**, 64 (2016).
 44. Yoshinaga, N., Nagai, K. H., Sumino, Y. & Kitahata, H. Drift instability in the motion of

- a fluid droplet with a chemically reactive surface driven by Marangoni flow. *Phys. Rev. E* **86**, 016108 (2012).
45. Kasuo, Y., et al. Start of micrometer-sized oil droplet motion through generation of surfactants. *Langmuir* **35**, 13351–13355 (2019).
 46. Drescher, K., et al. Dancing Volvox: Hydrodynamic bound states of swimming algae. *Phys. Rev. Lett.* **102**, 168101 (2009).
 47. Zhang, H. P., Be'er, A., Florin, E.-L. & Swinney, L. Collective motion and density fluctuations in bacterial colonies. *PNAS* **107**, 13626–13630 (2010).
 48. Sanchez, T., Chen, D. T. N., DeCamp, S. J., Heymann, M. & Dogic, Z. Spontaneous motion in hierarchically assembled active matter. *Nature* **491**, 431–435 (2012).
 49. Maass, C. C., Krüger, C., Herminghaus, S. & Bahr, C. Swimming droplets. *Annu. Rev. Condens. Matter Phys.* **7**, 171–193 (2016).
 50. Cira, N. J., Benusiglio, A. & Prakash, M. Vapour-mediated sensing and motility in two-component droplets. *Nature* **519**, 446–450 (2015).
 51. Karpitschka, S., Liebig, F. & Riegler, H. Marangoni contraction of evaporating sessile droplets of binary mixtures. *Langmuir* **33**, 4682–4687 (2017).